Turkish Journal of Engineering
https://dergipark.org.tr/en/pub/tuje
e-ISSN 2587-1366

Optimizing Abrasive Water Jet Parameters for Enhanced Interactivity in Metal-Stacked Hybrid Fiber Laminates

K. Gnanasekaran[1], M. Rajesh[*1], V. Hariram[1]
[1]*Hindustan Institute of Technology and Science, Department of Mechanical Engineering, Chennai – 603103,* gnanasekaran2007*@gmail.com; mvrajesh1991@gmail.com; connect2hariram@gmail.com*

Cite this study: Gnanasekaran, K., Rajesh, M., & Hariram, V. (2025). Optimizing Abrasive Water Jet Parameters for Enhanced Interactivity in Metal-Stacked Hybrid Fiber Laminates. Turkish Journal of Engineering, 9 (1), 28-36.

https://doi.org/ 10.31127/tuje.1503990

Keywords
Titanium, Jute, Kevlar, Pressure, Abrasive, Kerf, Roughness.

Research Article

Received:24.06.2024
Revised:22.07.2024
Accepted:23.07.2024
Published:0.01.2025

Abstract

High strength and shock-absorbing hybrid Fibre Laminate (HFL) machining is required to get the required geometric shape and size and to test the functioning under various impact protection circumstances. The compression molding process was adopted to fabricate the HFL. Skin titanium metal and alternately interlaced durable jute and high strength Kevlar fiber. A Central Composite Design (CCD)-Response Surface Technique (RST) was used to conduct the experiments with varying abrasive water jet parameters like WP-water pressure, TS-traverse speed, SOD-stand-off distance, and AQ-abrasive quantity. The desirability optimization technique adopted to minimize the surface roughness (Ra) and kerf angle (KA). An experimental examination shows that when water jet pressure was raised to its maximum value, the Ra and KA considerably reduced by 28.69% and 8.25%, respectively. Similar to how the Ra and KR significantly reduced by an extent of 7.4% and 3.5% when the abrasive quantity was increased to its higher value. However, when SOD and TS increased, a reversal impact on Ra and KA was seen. According to surface topology study, the brittle fracture occurs with micro-chipping, and for the kevlar fiber, bulk machining.

1. Introduction

A useful structural material constructed of skin-thin metal sheets with interior patterns of fibre stacking is called hybrid fibre laminate (HFL). High impact absorption, exceptional wear, and fatigue are just a few of the unique properties of metal and polymer infused fibre that are shown by HFL [1–3]. HFLs have drawn several high-tech industrial components, such as the frames of cars, ships, and aeroplanes [4–7]. Until now, many varieties of HFL, including (titanium/carbon) and PEEK/Ti,Ti/Basalt/Flax have been developed particularly for shock-absorbing constructions [8–11]. However, research aims to use HFLs in an extremely difficult context of shock resistance that consistently occurs at a larger level [11,12]. The performance of composite depends upon the stacking sequence [13–16]. This is accomplished by using natural jute fibre, which is an acceptable substitute for glass fibre. It exhibits sufficient mechanical strength and thermal resistance, as well as strong chemical stability, resistance to environmental reactions, and non-combustibility behavior [17,18]. A natural Kevlar fibre was used to give a structural damping feature because to its superior shock absorption and strength characteristics [19,20]. A popular structural material with a high strength and bending strength is titanium alloy [21,22]. In order to satisfy the requirements of diverse applications, HFL must be machined into a variety of forms and sizes. However, machining is a difficult operation because, in contrast to homogenous materials, its cutting mechanism is complicated [23]. The mix of Ti, jute, kevlar, and Ti makes the machining process even more difficult. The use of standard machining techniques is limited by the poor heat conductivity and high stiffness of Ti [24], as well as the abrasive properties of jute fiber. In order to process exotic and novel materials, it is crucial to investigate unconventional material processing methods such abrasive water jet beam technological, EDM, Laser beam machining, and ultrasonic machining [25–29]. Preparing nonconductive hierarchical structures of materials like HFL is often advised using abrasive water jet machining (AWJM). For difficult-to-machine materials like titanium and composite laminate materials, AWJM is the coolest machining method available [30,31]. This method gets rid of the limitations of traditional

processing of the materials mentioned above—tool wear and thermal stress—potentially boosting the flexibility of AWJ machining [32]. Additionally, this procedure offers numerous clearly visible benefits, such as sophisticated profile trimming and no noise during processing. These characteristics are employed to assess the caliber of treated materials and verify the machining process parameters. Demiral et al. [33] demonstrated that employing high abrasive pressure (AP) with a low traverse speed and a small nozzle distance (ND) can result in a favorable jet profile and improve surface quality. Schwartzentruber et al. [34] conducted an experiment to examine the impact of several factors, including the diameter of the mixing tube, the rate at which abrasive is supplied (AQ), the pressure of the abrasive (WP), the distance between the nozzle and the material (SOD), the orientation of the fiber plies, and the speed at which the cutting tool moves (TS), on the cutting process of a CFRP laminate using abrasive pressure (AP). Based on the results, increasing the abrasive quantity rate (AQ) results in enhanced surface quality. The latest HFL design increases strength and internal shock energy absorption by sandwiching layers of dampening kevlar and high strength jute between Ti sheets. The machinability investigations of Ti/K/J/K/J/K/J/K/J/K/Ti HFL are becoming more significant in the adaptation of appropriate conditions in light of modifications to HFL design and various fibre layering features. Additionally, Ti/K/J/K/J/K/J/K/J/K/Ti HFL hasn't been investigated using any kind of non-traditional machining techniques yet. As a result, this research examines how AWJM process factors affect quality traits and details the method by which Ti/K/J/K/J/K/J/K/J/K/Ti HFL material is removed. Trials for the machining experiment were carried out using a CCD-RST.For certain machining settings, the response surface model was developed to reduce surface roughness (Ra) and kerf angle (KA).

2. Materials and Methods

Due to its superior all-around performance in a variety of weight reduction applications, Ti6Al4V alloy (Grade-V) sheet was chosen. Jute and Kevlar textiles with a bi-directional weaving pattern were utilised in this work to provide the HFL laminate the necessary qualities. The Sai Sakthi India Corporation provided these fabric fabrics for commercial use. The kevlar, jute, and Ti sheets that were delivered had respective thicknesses of 0.5, 0.42, and 0.24 mm. The Ti sheet's surface becomes rougher as a result of this procedure, and residual stress is also added. The Ti sheet was then subjected to an annealing procedure in a muffle furnace to eliminate any generated residual tensions. A sheet of titanium was heated to 500°C for one hour and then submerged for six hours. The sheet was then cooled under conditions of ambient air and temperature. The surface of a Ti sheet was examined using a SEM and EDX before and after it had been annealed and subjected to sand blasting [35]. As received, the Ti surface is coated with a layer of ambient species that have been adsorbed, as can be seen in Figure. 1, which results in a dull SEM picture. The surface irregularity on the Ti sheet was evident in the SEM picture after sand blasting, as illustrated in Figure. 2. By comparing EDX profiles, it was possible to see constitutional alloying constituents of the Ti4Al6V alloy as well as a rise in the oxygen mass percentage for sand-blasted Ti sheet from 4.21 to 31.89. The present HFL design was created by stacking interlayers made of various fabrics like jute and kevlar in between sheets of titanium. First, a 3-hour chemical treatment in a 5% sodium hydroxide alkaline solution was performed on Kevlar fiber. The interfacial connection between fibres and polymer is anticipated to strengthen as a result of these chemical treatments. Compression moulding was used to create Ti/K/J/K/J/K/J/K/J/K/Ti HFL. As a polymer resin and curing agent, hardener and epoxy resin were used in a 10:1 ratio [14]. To make it simple to remove the processed laminate from the mould cavity, a thin waxy covering was first placed to all of its surfaces. According to the stack design, a substitute layer of three jute and two kevlar textiles was constructed on the mould cavity in between two Ti sheets. The resin was put between the layers before layer building and squeezed using a steel roller. This procedure removes any air pockets in the HFL laminate and considerably boosts resin penetration into fibre materials. It was then allowed to cure for 24 hours at room temperature. The laminate underwent post-curing for three hours at 70°C in order to enhance cross-linking. The fabricated hybrid Fibre Laminate (HFL) had a thickness about 6 mm, dimensions of 300 mm by 250 mm, and a density (q) of 1.945 g/cm^3. Table 1. Shows the Properties of Ti sheet, Jute, and Kevlar fiber respectively.

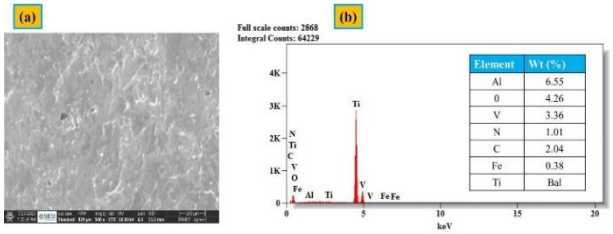

Figure 1. (a) SEM (b)EDX of Received Ti

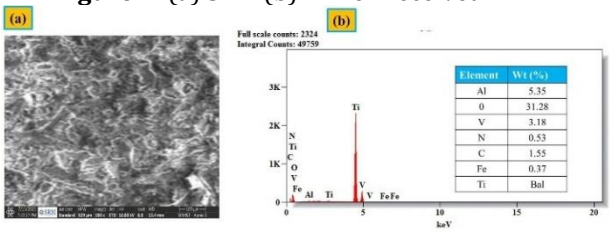

Figure 2. (a) SEM (b)EDX of Treated Ti

Table 1. Properties of Ti sheet, Jute, and Kevlar fiber [19,31]

Properties	Titanium	Kevlar	Jute
Density (g/cm^3)	4.43	1.4	1.3
Tensile modulus (GPa)	113	62	26.5
Tensile strength (MPa)	950	2758	393-773

2.1 Experimental Procedure

A three-axis MAXIEMA AWJM machine was used to experiment with machining on the manufactured HFL. The water pump is capable of producing pressures up to 450 MPa. Some of the AWJM settings were adjusted to a constant value to permit cutting operation. The orifice is sapphire with a diameter of 0.32 mm, garnet mesh size is 80 (an equivalent ASTM grain size is 177 µm), mixing tube diameter is 0.622 mm, nozzle diameter is 1 mm, and the jet angle is 90° [32]. The HFL's complete straight-line slot was carved in a single pass. Figure. 3 displays an AWJM setup and a typical machined HFL laminate. The experiments for minimizing surface roughness (Ra) and kerf angle (KA) during machining on Ti/K/J/K/J/K/J/K/J/K/Ti HFL were built and modelled using the RST-CCD approach.

Table 2. Experimental machining parameters

Process parameters	-2	-1	0	1	2
WP (MPa)	150	180	230	270	`310
SOD (mm)	1.5	2	2.5	3	3.5
AQ (g/min)	130	180	230	280	330
TS (mm/min)	110	135	160	185	210

Table 3. CCD-DOE order with response results

Run order	WP, MPa	SOD, mm	TS, mm/min	AQ, g/min	Ra, µm	KA, degree
1	230	230	160	2	4.08	1.77
2	150	130	210	1.5	5.01	2.12
3	310	130	110	1.5	3.31	1.41
4	190	230	160	2.5	4.71	2.03
5	150	330	110	3.5	4.23	1.87
6	150	130	110	1.5	4.89	2.07
7	310	130	210	3.5	3.64	1.55
8	230	280	160	2.5	3.92	1.67
9	150	330	210	1.5	4.17	1.82
10	310	330	210	1.5	3.15	1.32
11	230	230	135	2.5	4.02	1.71
12	310	330	110	3.5	3.18	1.37
13	310	330	210	3.5	3.43	1.43
14	150	330	210	3.5	4.73	2.05
15	310	130	210	1.5	3.56	1.51
16	270	230	160	2.5	3.82	1.62
17	150	330	110	1.5	3.77	1.59
18	230	230	160	3	4.49	1.92
19	150	130	210	3.5	5.14	2.15
20	310	330	110	1.5	3.12	1.24
21	150	130	110	3.5	4.97	2.09
22	230	230	185	2.5	4.26	1.89
23	230	180	160	2.5	4.54	1.95
24	310	130	110	3.5	3.48	1.47

The WP, TS, SOD, and AQ AWJM factors were taken into consideration for the experiment. Trial and error testing as well as earlier research reports on the machining of different laminates served as the foundation for the development of AWJM parameters and their ranges. The AWJM process variables and their levels are shown in Table 2. A video measuring approach was used to capture the kerf width at the top and bottom of the AWJM slot, as shown in Figure. 4 (a). The kerf dimension captured by the video measuring equipment at increased magnification. The angle between the top and bottom measured values of the kerf width was used to compute the kerf angle. The Surtronic S-128 meter was used to assess the Ra of the machined surface shown in in Figure. 4 (b). The cutoff length for recording surface roughness was chosen at 0.7 mm. At the plies' interface in the laminate thickness portion, surface roughness was measured. To reduce experimental error, three machining experiments were carried out in the prescribed manner and average of three trials. As shown in Table 3, Ra and KA were HFL machining output responses that represented quality attributes for certain cutting situations. Table 4 and 5 shows the ANOVA analysis of Ra and KA.

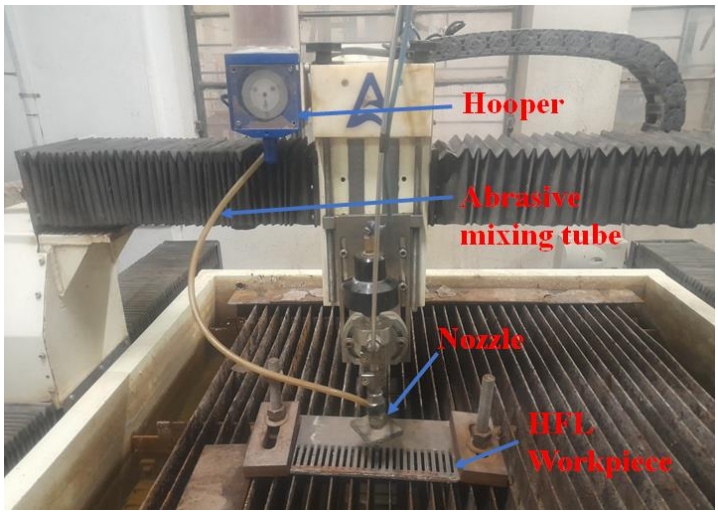

Figure 3. AWJM setup with metal fiber laminate

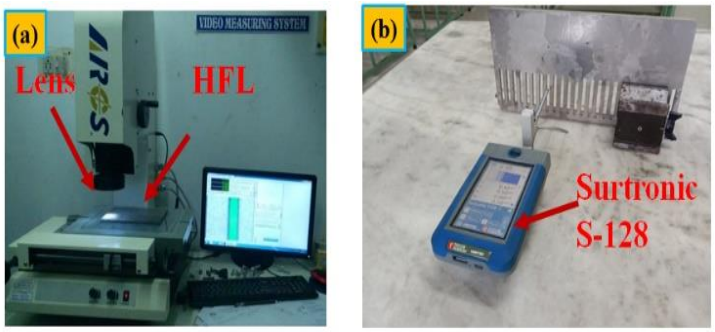

Figure 4. (a) Kerf width video measuring system and (b) Roughness Measurement

Table 4. ANOVA of surface roughness (R_a)

Source	SS	Df	MS	F-value	p-value
Model	1.63	4	0.4074	40.81	< 0.0001
WP	1.32	1	1.32	132.1	< 0.0001
SOD	0.2008	1	0.2008	20.11	0.0003
TS	0.0524	1	0.0524	5.25	0.0335
AQ	0.0576	1	0.0576	5.77	0.0267
Residual	0.1897	19	0.0100		
Cor total	1.82	23			
				R^2	0.8957
Std. Dev.	0.2208		R^2 -Adjusted		0.873
Mean	4.07		R^2- Predicted		0.840
C.V.%	5.43		Adequate precision		22.79

Table 5. ANOVA of kerf angle (KA)

Source	SS	Df	MS	F-value	p-value
Model	8.40	4	2.10	43.05	< 0.0001
WP	6.66	1	6.66	136.64	< 0.0001
SOD	1.24	1	1.24	25.51	< 0.0001
TS	0.2424	1	0.2424	4.97	0.0380
AQ	0.2485	1	0.2485	5.10	0.0359
Residual	0.9265	19	0.0488		
Cor total	9.32	23			
				R^2	0.9928
Std. Dev.	0.0999		R^2 -Adjusted		0.9899
Mean	1.73		R^2- Predicted		0.9834
C.V.%	5.76		Adequate precision		77.1512

3. Discussion

3.`1 Evaluation of RSM Model

As a function of several input process factors including WP, SOD, TS, and AQ, the Response Surface Model (RSM) has assisted in the construction of the mathematical models of Ra and KA. In order to eliminate the irrelevant interaction terms, the backward elimination approach was used [32]. Equations 1 and 2 provide the final quadratic response models for (KA) and (Ra) in terms of coded factors.

$$Ra=1.01241+0.0214884*WP+0.397661*SOD+0.02753*TS-0.00147*AQ \quad (1)$$

$$KA=2.02701+0.012456*WP+0.035781*SOD+0.001241*TS-0.00047*AQ \quad (2)$$

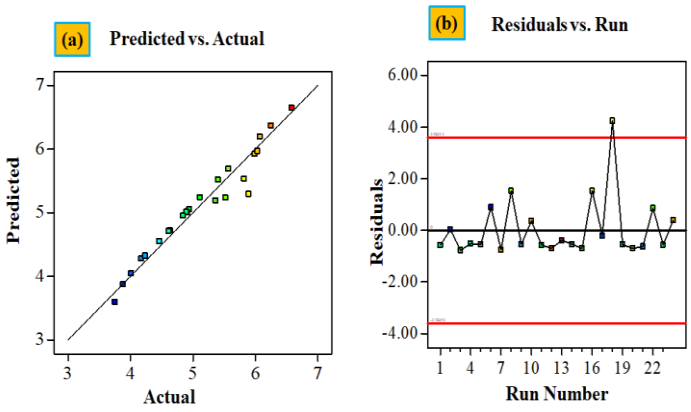

Figure 5. (a) Predicted Vs Actual; (b) Residuals vs. Run

Analysis of variance statistics (ANOVA) is used to evaluate the important process parameters. The findings of Ra and KA are shown in Tables 4 and 5. Ra's anticipated R^2 and corrected R^2 are estimated to vary by 0.0125 and 0.0232, respectively. These numbers are fewer than 0.2, indicating that the resulting model fits experimental data well and may be trusted to be utilized for interpolation. The signals to noise angle, which is often more than 4, serves as a representation of the accuracy of produced models in terms of sufficiency. According to the ANOVA findings, the minimal degree of an influence of noise is indicated by Ra's appropriate precision value of 75.1512 and KA's value of 62.30, which is larger than 4. The degree to which actual experimental data match in with the created response models is shown in Figure. 5(a, b). It demonstrates how the projected models and the experimental data are consistent.

3.2 Analysis on Ra

The ANOVA findings show that WP, which contributes 72.6% of the Ra, is the most important parameter, followed by TS (13.8%), SOD (3.98%), and AQ (3.57%). Additionally, several important interactions between the WP, TS, AQ, and SOD were found. A 3D surface plot for Ra as a function of the WP and AQ parameters is shown in Figure. 6 (a).

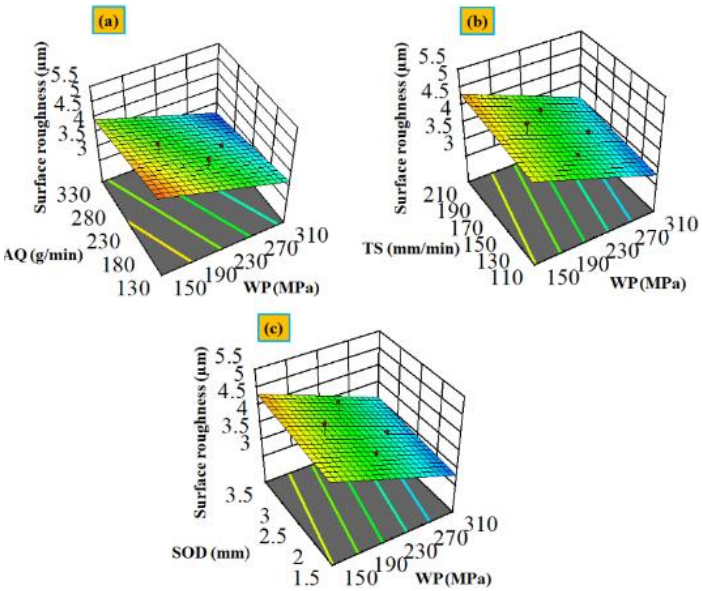

Figure 6. Parameter interaction effects on Ra

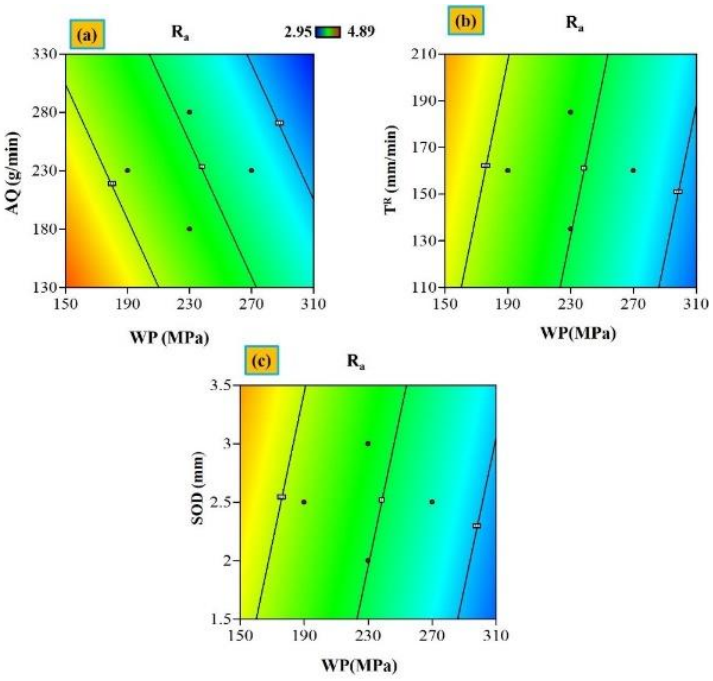

Figure 7. Contour effects on Ra

It demonstrates that at a greater level of WP of 320 MPa, the Ra value reached a minimum [32]. In contrast, Ra variation receives a larger value of 4.82 µm when WP and TS are both at low and high levels. The Ra achieved its greatest value of 4.01 m at a greater WP and TS, as seen in Figure. 6 (b). In the range of 175 mm/min, at constant AQ 150 g/min, WP 240 MPa, and SOD2 mm (middle level), the impact of SOD on the Ra was examined. Surface roughness was seen to rise by 7.35% when SOD was changed from a low setting value of 1.5 mm to a higher setting value of 3 mm [31]. The water jet beam diverges as a consequence of an increase in SOD, which lowers the kinetic energy of abrasive particles impacting the laminate cutting surface. Uneven cutting on Ti/CFRP/Ti HFL is a result of an increase in SOD [36]. However, it's possible to get a smoother cut surface with a low quantity of SOD. It creates precise streams of water jet with high-energy abrasive particles that erode the machining area smoothly and leave very light machining markings. As demonstrated in Figure. 6 (c), Ra value is found to be low at a greater AQ of 250 g/min compared to 50 g/min. The parametric condition of SOD of 2mm and WP of 320 MPa produced the lowest result of 3.14 µm. It is important to remember that the Ra marginally fell by 6.50% when the AQ went from low to high. Figure 7 (a-c) shows the contour plots of all interaction parameters [31].

3.3 Analysis on KA

Due to depletion of energy in the thickness orientation, the abrasive water jet's cutting performance deteriorates, and as a result, taper inclination develops on the kerf slot. The WP is the most significant parameter, contributing the maximum percentage of 74.7% to the ANOVA of KA, subsequent to AQ.

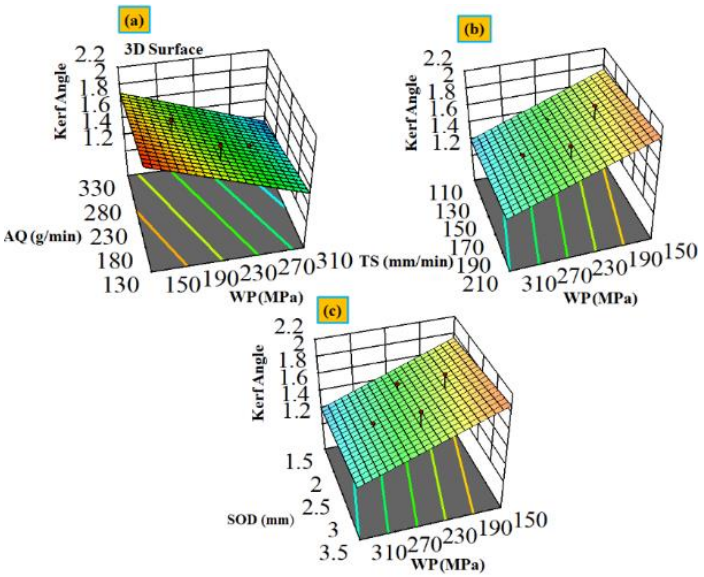

Figure 8. Parameter interaction effects on KA

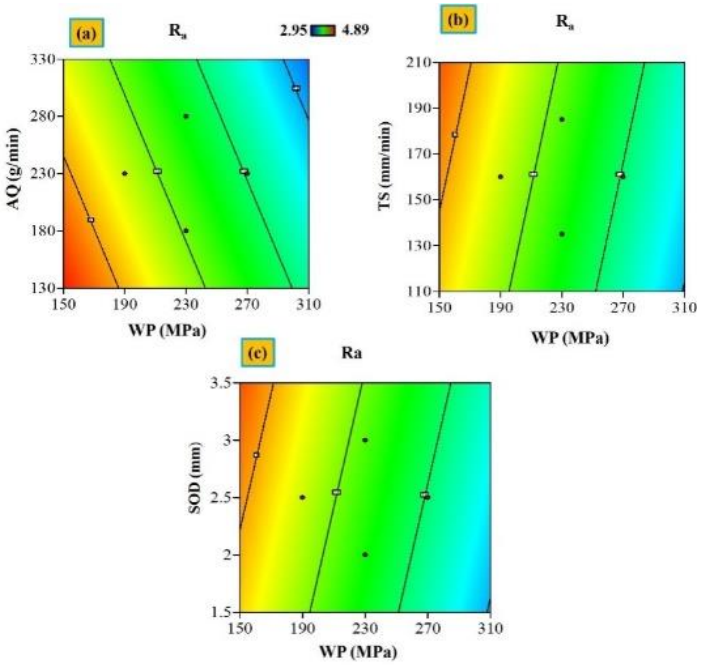

Figure 9. Contour effects on KA

It is significant to notice that the water jet velocity parameter is primarily involved in the variable interaction [37]. The KA value was low at an elevated WP of 310 MPa, as shown in Figure. 8 (a). However, when the interaction variable AQ is at the high level of 330g/min, the KA reaches its greatest value of 1.24 at a WP of 150 MPa. The Figure for KA is the lowest (1.07), with a WP of 310 MPa and a SOD of 1.5 mm. By changing the WP via 150 MPa to 310 MPa, the impact of the WP on KA is examined. According to Figure. 8(b), the kerf angle was at its maximum when the interaction parameter, WP, was set to 160 MPa and the TS was 225 mm/min. In an interval of 110 to 210 mm/min, at constant an influence of TS was examined. It was found that the KR rose by up to 3.44% when the TS climbed from 110 mm/min to 210 mm/min [36]. The greater KA reading of 1.22 was attained at a lower threshold of AQ and WP parameters [32], as shown in Figure. 8(c). However, when SOD and WP were increased, it fell to 1.08 µ. In order to

demonstrate how AMFR affects KR, AQ is thought to be adjusted from 1-3 mm while maintaining constant levels of all intermediate level parameters. Figure 9 (a-c) shows the contour plots of all interaction parameters [31].

3.4 Mechanisms of Erosion

Due to varied material conditions in the thickness direction, the manufactured HFL displays heterogeneous material behavior, making it difficult to determine the removal process. The machining characteristics and methods of material removal were examined using the SEM images from the different locations of the HFL machined surface. To further understand the machining behavior of HFL Figure 10(a), SEM studies were conducted at the interfaces of Ti/jute, jute/kevlar, and jute/Ti.

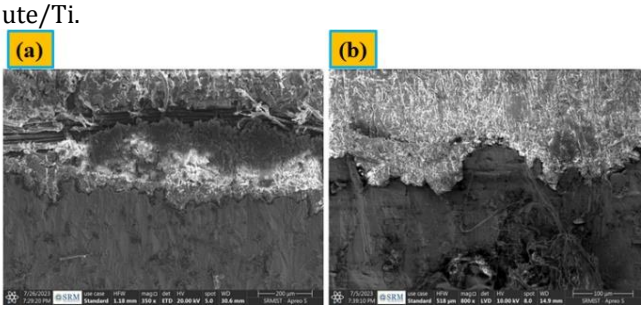

Figure 10. SEM images of AWJ machined surface

Figure 10(b) displays SEM images of the top portion of the Ti/jute interface at high and low water jet pressure settings. By comparing micrographs, it can be shown that greater pressures provide a smoother cut surface without an edge burr [31]. A water jet outer border without distortion is often produced by a high-water jet pressure. It has been determined that both operating situations used the identical material removal processes. The size of surface feature markers, which is large under low water pressure circumstances, was the only thing that differed. The alternately existing jute/Kevlar fibre inter-plies are exposed to abrasive water jet machining as the water jet advances in the thickness direction. The water jet energy is used to cleave the Ti/jute contact before being absorbed by the kerf wall and abrasive particle collisions [32].

3.5 Desirability analysis

The HFL machining performance may be improved by adopting optimization approach [32,38,]. The target's goal is to reduce the AWJM reactions of Ra and KA by taking into account a number of input factors, including AQ, WP, TS, and SOD. A composite desire function analysis, one of the methodologies, forecasts the process performances and product quality via the use of a dimensionless assessment system [31]. In order to priorities the available process parameters, this method translates process responses into the necessary dimensionless desirability function value (df), as illustrated in equation (3) [36].

$$d_f = \left[\frac{Max_i - R_i}{Max_i - Min_i}\right]^{w_i} \quad (3)$$

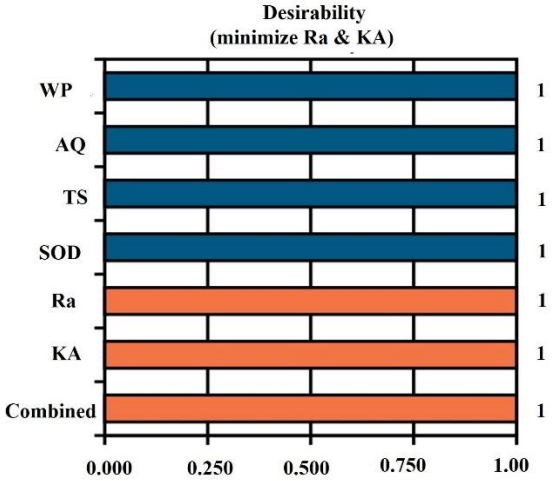

Figure 11. Bar graph

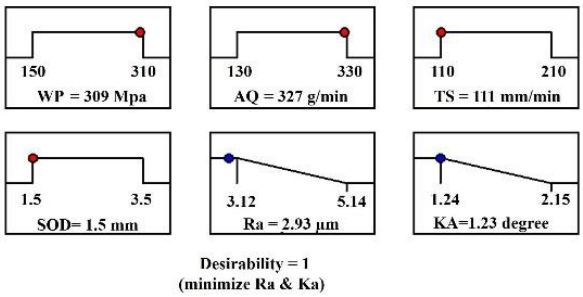

Figure 12. Ramp plot

This figure displays the response surface's contour as determined by the RST method. High WP and AQ have supported the reduction of Ra and KA, whereas TS and SOD show the opposite tendency. The desirability analysis bar graph, as shown in Figure 11, illustrates the relative desirability value of the supplied input parameters and responses to the objective aim. Figure 12 illustrates how the ramp function predicts the optimized values. These parameters, which are most suited to obtaining the lowest Ra and KA, are SOD, 2.5 mm; WP, 230 MPa; TS, 185 mm/min; and AQ, 230 g/min.

3.6 Confirmation

Validation experiments were carried out in a variety of process input variables in order to verify the projected outcomes of RST models with real experimental findings. The results are shown in Table 6. Utilizing the factors listed in Table 6 and the average of three trials, the actual experimental results were determined. It is shown that confirmation trials show an error between the actual experimental and projected values of less than 5% [31] . Therefore, the Ti/K/J/K/J/K/J/K/J/K/Ti stacked hybrid fibre laminate (HFL) AWJM may be performed using the proposed RST models.

Table 6. Confirmation results of Ra and KA

WP, MPa	150	230	230
SOD, mm	1	2.5	2.5
TS, mm/min	210	185	185
AQ, g/min	230	230	230
Ra (μm)- Predicted	5.21	4.12	3.91
Actual	5.10	3.98	3.87
Error	2.14	3.39	1.00
KA- Predicted	2.75	1.76	1.46
Actual	2.85	1.78	1.46
Error	3.63	1.13	4.48

4. Conclusions

AWJM was used machine the Ti/K/J/K/J/K/J/K/J/K/Ti stacked hybrid fibre laminate (HFL) with high strength and environmental friendliness. To determine the influencing process factors and their impact on machining characteristics, the RST optimization with desirability evaluation was carried out.

1. Using ANOVA statistics, it was possible to carefully examine how much influence various process factors had on the reduction of (KA) and (Ra). The (KA) and (Ra) were found to be significantly influenced by the water jet pressure (WP), contributing 73.5% and 82.6%, respectively.
2. According to experimental findings, the water jet pressure (WP) greatly lowers both the (KA) and (Ra). This is due to the Ti sheets and fibers bundle being eroded more evenly in the water jet penetration direction due to the highjet energy and increased abrasive particle flow per unit time.
3. To reduce the KR and, the RST technique optimized the AWJM parameters of WP 230 MPa, TS 185 mm/min, SOD 2.5 mm, and AQ 230 g/min.
4. The material removal process of the Ti/jute/kevlar/Ti HFL was validated by SEM analysis, which revealed brittle fracture of the jute fibre ply, bulk machining of the kevlarfibre ply, and ductile machining with microscopic plastic ploughing in the Ti ply.

Acknowledgement

This work was supported by the Hindustan Institute of Technology and Science, Padur, Chennai-603103 [SEED/CRC/HITS/2022-23-008].

Author contributions

K Gnanasekaran: Experimentation, validation and Editing
M Rajesh: Supervision, Modelling, Experimentation and Writing- Original draft .
V Hariram: Methodology, Reviewing and Editing.

Conflicts of interest

The authors declare no conflicts of interest.

References

1. Etri, H. E., Korkmaz, M. E., Gupta, M. K., Gunay, M., & Xu, J. (2022). A state-of-the-art review on mechanical characteristics of different fiber metal laminates for aerospace and structural applications. The International Journal of Advanced Manufacturing Technology, 123(9), 2965-2991.
2. Costa, R. D. F. S., Sales-Contini, R. C. M., Silva, F. J. G., Sebbe, N., & Jesus, A. M. P. (2023). A Critical Review on Fiber Metal Laminates (FML): From Manufacturing to Sustainable Processing. Metals, 13, 638.
3. Krishnakumar, S. (1994). Fiber Metal Laminates — The Synthesis of Metals and Composites. Materials and Manufacturing Processes, 9, 295–354.
4. Sherkatghanad, E., Lang, L., Blala, H., Li, L., & Alexandrov, S. (2019). Fiber Metal Laminate Structure, a good replacement for monolithic and composite materials. IOP Conference Series: Materials Science and Engineering, 576, 012034.
5. Ali, A., Pan, L., Duan, L., Zheng, Z., & Sapkota, B. (2016). Characterization of seawater hygrothermal conditioning effects on the properties of titanium-based fiber-metal laminates for marine applications. Composite Structures, 158,199–207
6. Blala, H., Lang, L., Khan, S., Li, L., Sijia, S., Guelailia, A., Slimane, S. A., & Alexandrov, S. (2023). Forming challenges of small and complex fiber metal laminate parts in aerospace applications—a review. The International Journal of Advanced Manufacturing Technology, 126, 2509–2543.
7. Etri, H. El, Korkmaz, M. E., Gupta, M. K., Gunay, M., & Xu, J. (2022). A state-of-the-art review on mechanical characteristics of different fiber metal laminates for aerospace and structural applications. The International Journal of Advanced Manufacturing Technology, 123, 2965–2991.
8. Ding, Z., Wang, H., Luo, J., & Li, N. (2021). A review on forming technologies of fibre metal laminates. International Journal of Lightweight Materials and Manufacture, 4,110–126.
9. Dhar Malingam, S., Jumaat, F. A., Ng, L. F., Subramaniam, K., & Ab Ghani, A. F.(2018). Tensile and impact properties of cost-effective hybrid fiber metal laminate sandwich structures. Advances in Polymer Technology, 37, 2385–2393.
10. Giridharan, D., & Rakham, B. (2018). Experimental Analysis of Fibre Metal Laminates. IOP Conference Series: Materials Science and Engineering, 455: 012037.
11. Chen, Y., Wang, Y., & Wang, H. (2020). Research Progress on Interlaminar Failure Behavior of Fiber Metal Laminates. Advances in Polymer Technology, 2020(1), 3097839.
12. Serubibi, A., Hazell, P. J., Escobedo, J. P., Wang, H., Oromiehie, E., Prusty, G. B., Phillips, A. W., & St John, N. A. (2023). Fibre-metal laminate structures: High-velocity impact, penetration, and blast loading – A review. Composites Part A: Applied Science and

Manufacturing, 173, 107674.
13. Kirubakaran, R., Kaliyamoorthy, R., Munusamy, R., & Annamalai, B. (2023). Mechanical and vibration behavior of surface-modified titanium sheet interleaved with woven basalt/flax fiber metal laminates. Polymer Composites, 44, 8442–8453.
14. Ramraji, K., Rajkumar, K., & Sabarinathan, P. (2020). Mechanical and free vibration properties of skin and core designed basalt woven intertwined with flax layered polymeric laminates. Proceedings of the Institution of Mechanical Engineers, Part C: Journal of Mechanical Engineering Science, 234, 4505–4519.
15. Şimşek Türker, Y., & Kılınçarslan, Ş. (2024). Experimental and analytical investigation of the effect of layer number and thickness on the bending properties of glulam beams. Kahramanmaraş Sütçü İmam Üniversitesi Mühendislik Bilimleri Dergisi, 27, 141–150.
16. Özbek, Ö., Bozkurt, Ö., & Erklig, A. (2020). Low velocity impact behaviors of basalt/epoxy reinforced composite laminates with different fiber orientations. Turkish Journal of Engineering, 4,197–202.
17. Ramesh, M., Palanikumar, K., & Reddy, K. H. (2013). Mechanical property evaluation of sisal–jute–glass fiber reinforced polyester composites. Composites Part B: Engineering, 48,1–9.
18. Karacor, B., & Özcanlı, M. (2021). Different Curing Temperature Effects on Mechanical Properties of Jute/Glass Fiber Reinforced Hybrid Composites. International Journal of Automotive Science And Technology, 5, 358–371.
19. Yeter, E. (2019). Investigation of Ballistic Impact Response of Aluminum Alloys Hybridized with Kevlar/Epoxy Composites TT - Investigation of Ballistic Impact Response of Aluminum Alloys Hybridized with Kevlar/Epoxy Composites. Politeknik Dergisi, 22, 219–227.
20. Naveen, M. R., Kamaraj, L., & Ponnarengan, H. (2024). Adhesion strength and mechanical properties of nanoclay modified hybrid kevlar/jute-epoxy fiber metal laminate. Polymer Composites.
21. Wang, Y., Sun, W., & Cao, L. (2024). Tensile and flexural mechanical attributes of hybrid carbon/basalt fiber metal laminates under various hybridization and stacking sequences. Composites Part A: Applied Science and Manufacturing, 177, 107942.
22. Babaytsev, A., Lopatin, S., & Nasonov, F. (2024). Study of dynamic characteristics of hybrid titanium-polymer composite materials. International Journal for Computational Civil and Structural Engineering, 20, 109–115.
23. Debnath, K., Sisodia, M., Kumar, A., & Singh, I. 2016. Damage-free hole making in fiber-reinforced composites: an innovative tool design approach. Materials and Manufacturing Processes, 31, 1400–1408.
24. Xu, J., Zhou, L., Chen, M., & Ren, F. (2019). Experimental study on mechanical drilling of carbon/epoxy composite-Ti6Al4V stacks. Materials and Manufacturing Processes, 34, 715–725.
25. Ishfaq, K., Mufti, N., Ahmed, N., & Pervaiz, S. (2018). Abrasive waterjet cutting of cladded material: kerf taper and MRR analysis. Materials and Manufacturing Processes, 34, 1–10.
26. Xu, J., li, C., Chen, M., & Ren, F. (2019). A comparison between vibration assisted and conventional drilling of CFRP/Ti6Al4V stacks. Materials and Manufacturing Processes, 34,1182–1193.
27. Karthikeyan, M., Pandian, S. M. V., & Vijayakumar, R. (2023). Investigation on Metal Hybrid Fibres Laminate (MHFL) in hybrid machining. Journal of Manufacturing Processes, 101, 835–853.
28. Rao, S., Sethi, A., Das, A. K., Mandal, N., Kiran, P., Ghosh, R., Dixit, A. R., & Mandal, A. (2017). Fiber laser cutting of CFRP composites and process optimization through response surface methodology. Materials and Manufacturing Processes, 32, 1612–1621.
29. Şimşek, T., Baris, M., Ozcan, S., & Akkurt, A. (2019). Investigation of machinability properties of laser treated S355JR carbon steel with ZRB2 nanoparticles. Turkish Journal of Engineering, 3, 51–59
30. Kechagias, J., Petropoulos, G., & Vaxevanidis, N. (2012). Application of Taguchi design for quality characterization of abrasive water jet machining of TRIP sheet steels. The International Journal of Advanced Manufacturing Technology, 62, 635–643.
31. Rajesh, Munusamy, Kaliyamoorthy, R., & Kirubakaran, R. (2022). Parametric investigation on surface roughness and hole quality of Ti metal hybrid fibers cored laminate (MFL) during abrasive water jet drilling. Proceedings of the Institution of Mechanical Engineers, Part C: Journal of Mechanical Engineering Science, 236, 4147–4165.
32. Rajesh, M., Rajkumar, K., & Annamalai, V. E. (2021). Abrasive water jet machining on Ti metal-interleaved basalt-flax fiber laminate. Materials and Manufacturing Processes, 36, 329–340.
33. Demiral, M., Abbassi, F., Saracyakupoglu, T., & Habibi, M. (2022). Damage analysis of a CFRP cross-ply laminate subjected to abrasive water jet cutting. Alexandria Engineering Journal, 61, 7669–7684.
34. Schwartzentruber, J., Papini, M., & Spelt, J. K. (2018). Characterizing and modelling delamination of carbon-fiber epoxy laminates during abrasive waterjet cutting. Composites Part A: Applied Science and Manufacturing, 112, 299–314.
35. Kumar, D., & Gururaja, S. (2020). Abrasive waterjet machining of Ti/CFRP/Ti laminate and multi-objective optimization of the process parameters using response surface methodology. Journal of Composite Materials, 54, 1741–1759.
36. Dhanawade, A., Kumar, P., & Kumar, S. (2020). Experimental study on abrasive water jet machining of carbon epoxy composite. Advances in Materials and Processing Technologies, 6, 40–53.38.
37. Pahuja, R., & M., R. (2019). Abrasive water jet machining of Titanium (Ti6Al4V)–CFRP stacks – A semi-analytical modeling approach in the prediction of kerf geometry. Journal of Manufacturing Processes, 39, 327–337.

38. Çelik, İ., Yıldız, C., & Şekkeli, M. (2021). Wind power plant layout optimization using particle swarm optimization. Turkish Journal of Engineering, 5, 89–94.